Biochar & Compost Technology, 1(1), 56-71
10.21608/bct.2025.411461

Journal home page: https://bct.journals.ekb.eg/

Influence of Pyrolysis Temperature on the Adsorption Efficiency of Date Palm's Petiole Biochar for N and P in Aqueous Solutions

Bahaaeldein M. Khudairi[1*], Khaled M. Ibrahim[2], and Ahmed A. Abdelhafez[1]

[1] Department of Soils and Water Science, Faculty of Agriculture, New Valley University, El-Kharga 72511 Egypt (bahaaeldeenmahmoud@agr.nvu.edu.eg, ahmed.aziz@agr.nvu.edu.eg)

[2] Agronomy Department, Faculty of Agriculture, New Valley University, El-Kharga 72511 Egypt; K.elgeady@agr.nvu.edu.eg

***** Correspondence: bahaaeldeenmahmoud@agr.nvu.edu.eg; Tel.: (+2 01156744985).

ARTICLE INFORMATION

Received: 15 December, 2024, Received in revised form 30 January, 2025
Accepted: 5 February, 2025, Available online 13 February, 2025

ABSTRACT

The significant presence of nitrogen (N) and phosphorus (P) in wastewater poses considerable environmental challenges, including eutrophication and soil and water contamination. This research examines the adsorption efficacy of biochar produced from date palm petiole subjected to pyrolysis at temperatures of 300°C, 500°C and 700°C for the removal of nitrate (NO_3^-), ammonium (NH_4^+), and phosphorus (P) from aqueous environments. Characterization of the biochar revealed that increasing the pyrolysis temperature resulted in enhanced porosity, surface area, and carbon content, along with a decrease in oxygen-containing functional groups. The adsorption kinetics were most accurately represented by the pseudo-first-order model for both NO_3^- and P, whereas NH_4^+ followed a pseudo-second-order model, indicative of chemisorption processes. The biochar obtained at 700°C (BC-700) exhibited the highest adsorption capacities for NH_4^+ and P, attributable to its highly developed microporous structure and improved cation exchange capacity. Conversely, the removal of NO_3^- was limited across all biochar samples. The Freundlich isotherm model offered the most suitable representation of the adsorption data, indicating the presence of heterogeneous sorption sites. These results underscore the potential of pyrolyzed biochar as an environmentally sustainable adsorbent for nutrient removal from wastewater, with optimized pyrolysis conditions enhancing adsorption efficiency. However, additional investigations are warranted to augment the removal efficiency of nitrate through biochar modifications or the implementation of integrative treatment strategies.

Keywords: Biochar; Pyrolysis; Adsorption Kinetics; Nitrate; Ammonium; Phosphorus; Aqueous Solutions.

1. Introduction

The overabundance of nitrogen (N) and phosphorus (P) in wastewater presents considerable environmental challenges, primarily attributable to their contribution to eutrophication. When wastewater with elevated concentrations of these nutrients is discharged into aquatic environments, it incites the accelerated proliferation of algae and aquatic vegetation, resulting in algal blooms. The decomposition of these blooms consumes oxygen in the water, leading to hypoxic or anoxic conditions that can jeopardize the survival of aquatic organisms, including fish and invertebrates (Smith et al., 1999). Additionally, algal blooms have the potential to generate harmful toxins that pose risks to both aquatic ecosystems and human

health, particularly affecting sources of drinking water (Paerl et al., 2011). Furthermore, heightened nitrogen levels can lead to nitrate contamination in groundwater, which poses health risks to humans, particularly the onset of methemoglobinemia or "blue baby syndrome" in infants (Ward et al., 2005). Mitigating these risks necessitates the implementation of effective wastewater treatment methodologies aimed at diminishing nutrient loads and averting their adverse effects on ecosystems and public health. Biochar, a carbon-rich substance generated via the pyrolysis of biomass, has received considerable interest for its role in environmental remediation, especially in the recovery of nutrients from liquid solutions (Abdelhafez and Li, 2016). The efficacy of biochar in adsorption is greatly affected by its physicochemical characteristics, which are determined by the conditions of the pyrolysis process, with temperature being a particularly critical factor (Abdelhafez et al., 2020). Previous research has demonstrated that elevating the pyrolysis temperature influences the surface area, pore structure, and functional group composition of biochar, which in turn affects its adsorption properties (Ahmad et al., 2014; Akhtar et al., 2021). Generally, high pyrolysis temperatures lead to the formation of biochars characterized by increased surface areas and more developed pore structures, which improve their physical adsorption characteristics (Tan et al., 2015; Akhtar et al., 2021). Nevertheless, this process may also diminish the quantity of oxygen-containing functional groups, potentially decreasing the chemisorption capacity for specific nutrients such as nitrogen (Inyang et al., 2012).

The phenomenon of phosphorus (P) adsorption by biochar has been extensively studied, with investigations emphasizing the significance of particular interactions, including ligand exchange and precipitation involving minerals located on the biochar surface (Xu et al., 2013). For example, Xiao et al. (2024) illustrated that biochars produced from agricultural waste displayed enhanced P adsorption at moderate pyrolysis temperatures, attributable to an optimal equilibrium between surface area and the availability of functional groups.

In the context of nitrogen adsorption, ammonium ions (NH_4^+) are typically retained via cation exchange processes, which are modulated by the cation exchange capacity (CEC) of the biochar (Chen et al., 2008). Biochars generated at lower pyrolysis temperatures frequently exhibit elevated CEC values, attributable to the preservation of organic matter and functional groups (Gai et al., 2014). Conversely, at elevated pyrolysis temperatures, the reduction of volatile components and the development of aromatic structures may increase the stability of biochar, although this may detrimentally affect its efficiency in adsorbing nitrogen species (Liu et al., 2017). Biochar is increasingly acknowledged as a highly effective adsorbent for the extraction of nitrate (NO_3^-) from aqueous solutions, attributable to its porous architecture, substantial surface area, and capacity for ion exchange (Vijayaraghavan & Balasubramanian, 2021; Aghoghovwia et al., 2022). The efficacy of nitrate extraction is largely contingent upon the physicochemical characteristics of the biochar, which are themselves determined by the type of feedstock utilized and the conditions under which pyrolysis occurs. Research indicates that biochars derived from lower pyrolysis temperatures tend to possess a higher cation exchange capacity (CEC), thereby rendering them more proficient in nitrate retention through electrostatic interactions (Nan et al., 2021). Furthermore, the presence of functional groups, such as hydroxyl and carboxyl moieties on the biochar surface, facilitates enhanced adsorption of nitrate via mechanisms including hydrogen bonding and ligand exchange (Wang et al., 2021; Zhang et al., 2023). The modification of biochar with substances such as metal oxides or clay has been shown to augment its adsorption capabilities by increasing the accessibility of active sites and improving the affinity for nitrate (Wang et al., 2021; Zhang et al., 2023). Notwithstanding its considerable potential, challenges persist, including competitive adsorption with other anions (for example, sulfate and chloride) as well as the desorption of nitrate under fluctuating environmental conditions. These factors necessitate

further study to refine the utilization of biochar for nitrate removal in practical applications. Despite the extensive wealth of studies on biochar and its capacity for nutrient adsorption, significant gaps still remain in our understanding of the intricate interplay between pyrolysis temperature and the adsorption performance for both nitrogen and phosphorus under a variety of environmental conditions. This study builds upon the foundational work conducted by previous researchers and seeks to deliver a more nuanced and detailed understanding of how pyrolysis temperature can be effectively optimized to maximize the adsorption efficiency of biochar in different contexts. By delving into this complex relationship, we aim to uncover valuable insights that can inform practical applications, ultimately enhancing the effectiveness of biochar as a sustainable solution for nutrient management in agricultural systems.

2. Materials and Methods

2.1 *Biochar production*

Date palm's petiole was selected as biomass feedstock due to its abundance in Egypt, and its low cost. Fresh date palm petiole was collected, air dried, mechanically shredded and cut to small pieces of 5 cm length, and stored in plastic bags before undergoing a pyrolysis process that took place Three different temperature settings, 300, 500, and 700ºC, were selected for the pyrolysis process, each of which was held for 60 minutes in a muffle furnace. The resulting biochars were labeled as BC-300, BC-500, and BC-700, respectively. The produced biochars were then crushed and sieved to pass through a 1mm sieve. Once biochar was produced, it was stored in airtight glass containers until further use.

2.2 *Biochar characterization*

Chemical, physical and engineering analyses were performed for analyzing the produced biochars were performed following the description of Abdelhafez et al. (2014 and 2021). Elemental composition of the produced biochars was measured by using CHNOS elemental analyzer (Vario-E, Germany) for measuring C, H, N and S. Organic matter and ash contents were measured by using loss on ignition method. pH and electrical conductivity (EC) of biochars were examined using a 1:10 (w/v) biochar/deionized water.

Fourier transform infrared (FTIR) spectrometry was utilized to identify functional groups on biochars, with analyses performed on powdered samples mixed with KBr pellets in the 4000–400 cm^{-1} range. The spectral data were obtained in a wavelength range from 4000 to 400 cm^{-1} using Thermoscientific instrument (NICOLET IS 10-USA). Microscopic structures of biochars were examined using scanning electron microscopy (SEM), with samples gold coated in a sputter coater for conductivity using Jeol (JSM 5440LV Scanning Microscope, Japan) instrument. The weights of the produced biochars were measured before and after the pyrolysis treatment and density was estimated as a weight per unit volume of biochar. All of the biochars produced were characterized to determine their structural properties. The BET surface area and pore volume analysis were conducted using Quantachrome TouchWin v1.2 instrument. The sample was degassed at 300 °C for at least 2 h to remove moisture before conducting the adsorption experiment.

2.3 *Preparation of NO_3^-, NH_4^+ and P solutions*

In the experiments, stock solutions (1000 mg L^{-1}) for each were prepared by using ammonium sulfate $(NH4)_2SO_4$, potassium nitrate KNO_3 and potassium dihydrogen phosphate KH_2PO_4. The necessary dilutions for the desired concentrations of N (NO_3^- and NH_4^+) and P were prepared by the stock solutions the day before conducting the adsorption experiments.

2.4 *Batch adsorption studies*

Batch experiments were conducted to investigate the effects of sorebnt dosage, contact time and initial concentration on nitrgen (NO_3^- and NH_4^+) and phosphorus (P) sorption using BC-300, BC-500 and BC-700 and their efficiencies for removing contaminants from aqueous solutions. The experiments utilized a series of 50 mL capped plastic flasks for shaking the samples on a mechanical shaker. Time-course experiments were conducted for periods ranging from 5-180 min. after adding sorbents at a fixed rate of 1 g L^{-1} and 50 mg L^{-1} for each tested metal ions then mixtures were agitated. At specific time intervals 5, 15, 30, 60, 120 and 180 min. 5mL samples were extracted from the tubes. To investigate the adsorption efficiency of NO_3^-, NH_4^+ and P, adsorption experiments were designed to test the role of sorbent dosage on adsorption efficiency. Each biochar was immersed with 30mL of 50 mg L^{-1} NO_3^-, NH_4^+ or P solutions in a 50 mL centrifuge tube, with an average biochar weight of 0.5, 1, 2.5, 5 and 10 g L^{-1}. Each tube was placed in a rotary shaker set to 120rpm in a dark chamber at room temperature which was recorded the optimum shaking time for NO_3^-, NH_4^+ and P removal. The removal efficiency was then calculated using the following equations:

$$Removal\ (\%) = \frac{\mathrm{C0} - \mathrm{Ce}}{\mathrm{Ce}} \times 100$$

where, C0 is the concentration of the applied Fe ions and Ce is the metal ions concentration at equilibrium, respectively. Tested ions adsorbed (mg g^{-1}) on biochar was calculated for each sorbent by the following equation:

$$qe = (\mathrm{C0} - \mathrm{Ce}) \times V$$

where, qe is the amount of adsorbed ions (mg g^{-1}), V is the applied concentration of ions solution volume (L) and W is the adsorbent weight (g).

The well-controlled methodology provides insights into how key parameters of sorbent dosage, contact time and concentration influence ions sorption by tested materials, furthering understanding of their potential for efficiently removing tested ions from aqueous solutions.

2.4.1 Adsorption isotherms

Several isotherms were tested to understand the main mechanism beyond NO_3^-, NH_4^+ and P removal from aqueous solutions i.e., Freundlich and Langmuir models (Abdelhafez and Li, 2016).

The Freundlich model is as follows:

$$\mathrm{q}_e = K_F {C_e}^{1/n}$$

where q_e is adsorbed metal per adsorbent mass, K_F and n are empirical constants, and C_e is equilibrium concentration. Its linearize form is:

$$\log q_e = \log K + \frac{1}{n} \log C_e$$

The Langmuir model (Joo et al., 2010; Abdelhafez and Li, 2016) is:

$$q_e = \frac{Q_{\max} bC_e}{1 + bC_e}$$

where Q_{max} is the maximum adsorption capacity and b indicates binding affinity. Qmax and b were calculated from the linear plot of Ce/qe vs Ce.

The dimensionless separation factor RL predicts favorable/unfavorable adsorption (Tan et al., 2008):

$$RL = \frac{1}{1 + bC_e}$$

RL values imply: >1 unfavorable, 1 linear, 0-1 favorable, 0 irreversible.

2.4.2. Adsorption kinetics models

Pseudo-first order and pseudo-second order models were used to analyze the adsorption kinetics of NO_3^-, NH_4^+ and P onto biochars (Ho and McKay, 1999).

The pseudo-first order model is:

$$\log(q_e - q_t) = logq_e - \frac{K_1 \,.\, ads}{2.303} t$$

Where, q e and q t (mg g^{-1}) are the amount of metal ions adsorbed at equilibrium (mg g^{-1}) and t (mins), respectively, and K_1 is the rate constant of the equation ($mins^{-1}$).

The pseudo-second order model is:

$$\frac{dq}{dt} - \left(q_{eq-}q\right)^2$$

And integrating the equation yields as follows:

$$\frac{t}{q} - \frac{1}{K_{2adsqe^2}} + \frac{t}{q_e}$$

Where, *t* (min.) is the contact time, q_{eq} (mg g^{-1}) and q (mg g^{-1}) are the amount of metal ions adsorbed at equilibrium and at any time of reaction t.

2.5 Statistical analysis

A statistical analysis of the data was conducted utilizing a post-hoc test aimed at assessing specific differences between the treatments, employing Duncan's Multiple Range Test (DMRT). The significant differences among treatment means were evaluated through analysis of variance, with mean separation carried out at a significance level of 5% ($p \leqslant 0.05$). All graphical representations were generated using the Sigma plot software.

3. Results and Discussion

3.1 . Biohar characterization

Table 1. shows the chemical, physical and engineering characteristics of the produced biochars. The characteristics of biochar are markedly affected by the pyrolysis temperature throughout its synthesis. As the temperature escalates from 300°C to 700°C, several significant and consequential alterations take place: the pH level of biochar increases in alkalinity, advancing from 8.61 to 9.12. This observation is consistent with an array of studies indicating that elevated pyrolysis temperatures typically augment biochar alkalinity (Tomczyk et al., 2020). Furthermore, the carbon concentration experiences a substantial rise from 53.1% to 69.65%, while the proportions of hydrogen, nitrogen, sulfur, and oxygen decrease considerably, illustrating a heightened level of carbonization alongside a reduction in volatile compounds (Chatterjee et al., 2020). In terms of physical properties, the yield of

biochar declines drastically from 70.45% to 33.56% as the temperature increases, reflecting an amplified decomposition of the initial biomass occurring during the pyrolysis process (Khater et al., 2024). Additionally, the effects of elevated temperatures are evident in the enhancement of the BET surface area (from 0.018 m^2 g^{-1} to 0.051 m^2 g^{-1}) and pore volume (from 0.039 cm^3 g^{-1} to 0.06 cm^3 g^{-1}), which collectively improve the biochar's porosity and its potential for adsorption (Abdelhafez and Li, 2016; Chatterjee et al., 2020). These extensive modifications indicate that higher pyrolysis temperatures facilitate the generation of biochar with increased carbon content and enhanced porosity, albeit with a reduced overall yield, this is a critical consideration that can profoundly affect its applicability in essential functions such as soil improvement, pollutant adsorption, and effective carbon capture.

Table 1. Chemical, physical and engineering characteristics of the produced biochars

Parameter	Unit	BC-300	BC-500	BC-700
Chemical characteristics				
pH		8.61	8.92	9.12
EC	dS m^{-1}	0.86	0.8	0.78
C	%	53.1	64.76	69.65
H		1.21	0.75	0.48
N		0.38	0.221	0.14
S		1.48	1.12	0.87
O		0.83	0.649	0.36
OM	g kg^{-1}	570	677.5	715
Physical and engineering properties				
Loose on pyrolysis	%	29.55	45.66	66.44
Yield		70.45	54.34	33.56
Ash		43.0	32.5	28.5
Density	ton m^{-3}	0.188	0.212	0.238
BET surface area	m^2 g^{-1}	0.018	0.036	0.051
Average particle size	nm	156.1	24.62	16.91
Pore volume	cm^3 g^{-1}	0.039	0.054	0.06

As shown in Figure 1. The Fourier-transform infrared (FTIR) spectra of biochars generated at pyrolysis temperatures of 300°C (BC-300), 500°C (BC-500), and 700°C (BC-700) exhibit notable structural alterations correlated with the elevation of pyrolysis temperature. The extensive O-H stretching band (3200–3600 cm^{-1}) and the C=O stretching peak (approximately 1700 cm^{-1}), indicative of hydroxyl and carbonyl functional groups, are most pronounced in BC-300; however, their intensity diminishes at increased temperatures, signifying a continuous reduction of oxygen-containing functional groups (Zhao et al., 2017). Likewise, the aliphatic C-H stretching bands (approximately 2800–3000 cm^{-1}) progressively weaken with rising pyrolysis temperature, implying a transition from aliphatic to aromatic

configurations (Ahmad et al., 2014). In contrast, the C=C stretching vibrations (approximately 1500–1600 cm^{-1}), which are linked to aromatic structures, become increasingly pronounced in BC-700, indicating an enhancement in carbonization and aromaticity (Keiluweit et al., 2010). These observed trends are consistent with prior research indicating that elevated-temperature pyrolysis diminishes the occurrence of polar functional groups while promoting greater aromaticity and thermal stability (Xu et al., 2017). The Scanning Electron Microscopy (SEM) analysis of biochars derived from date palm petiole, subjected to pyrolysis at varying temperatures of 300°C, 500°C, and 700°C examined at a magnification of x10,000 reveals significant and notable morphological alterations that occur as the pyrolysis temperature is elevated. At the lower temperature of 300°C (Figure 2-A), the biochar largely preserves its fibrous plant structure, exhibiting limited pore formation, larger particle sizes, and signs of incomplete carbonization. This biochar retains attributes reminiscent of natural plant material, suggesting that the conversion into biochar is in its initial phases. Conversely, when the pyrolysis temperature is increased to 500°C (Figure2-B), the structural integrity of the biochar displays marked fragmentation, resulting in heightened surface roughness. This temperature promotes a significant development of pores and leads to a general reduction in particle size due to the enhanced efficiency of thermal decomposition occurring at this level. Lastly, at the elevated temperature of 700°C (Figure2-C), the biochar reveals highly porous structures characterized by well-defined micropores. Furthermore, a discernible trend of increased particle fragmentation is observed, along with a more organized carbon framework. This progression culminates in the attainment of optimal surface area and porosity characteristics. The overall observation indicates a clear correlation between higher pyrolysis temperatures and enhanced porosity, a reduction in particle sizes, and an increase in surface area (Akhtar et al., 2021). This establishes that biochar produced at 300°C may demonstrate greater stability for soil applications. In contrast, the biochar processed at the higher temperature of 700°C is more suitable for applications necessitating adsorption and filtration due to its exceptionally porous structure (Abdelhafez et al., 2016, Singh et al., 2024).

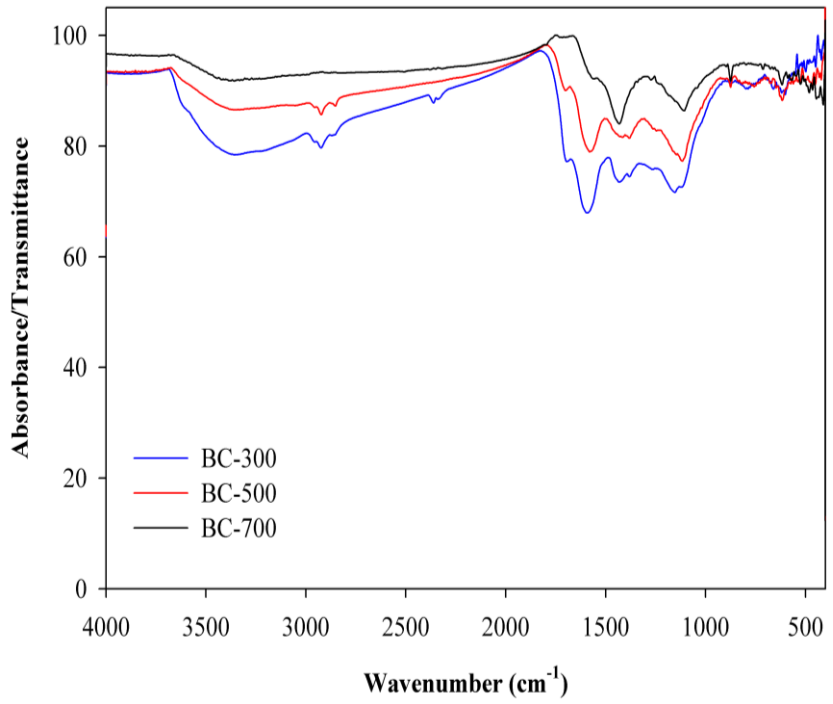

Figure 1. The Fourier-transform infrared (FTIR) spectra of biochars generated at pyrolysis temperatures of 300°C (BC-300), 500°C (BC-500) and 700°C (BC-700)

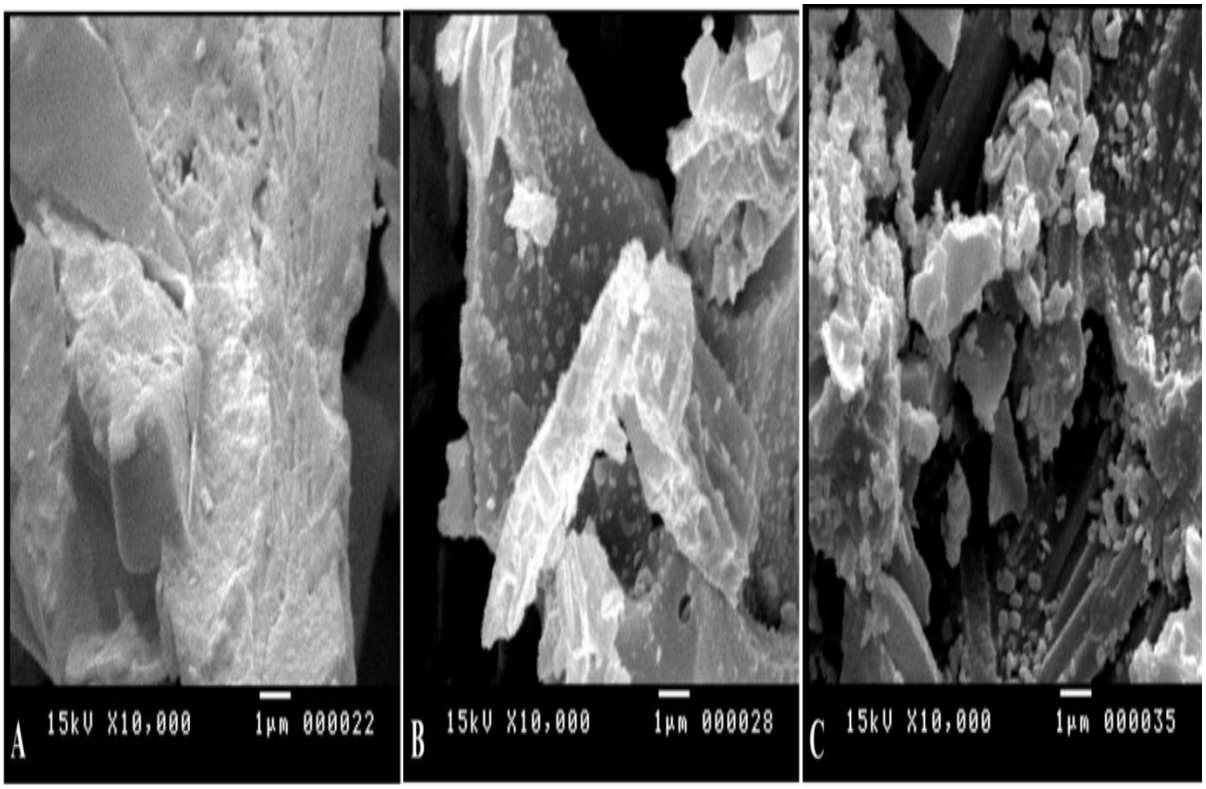

Figure 2. Scanning electron microscope (SEM) image of biochars derived from data palm petiole at different pyrolysis temperatures of 300°C (A), 500°C (B) and 700°C (C)

3.2 . Factors affecting sorption of NO_3^-, NH_4^+ and P by tested biochars

3.2.1. Contact time

Data presented in Figure 3 presents an analysis of the impact of contact duration (5-180 min.) on the removal efficiency of NO_3^-, NH_4^+, and P from aqueous solutions utilizing biochars generated at various pyrolysis temperatures (300°C, 500°C, and 700°C). The findings reveal that the removal efficiency of nitrate remains comparatively low for all types of biochar and across the tested contact durations, achieving a peak efficiency of approximately 18–20% at 180 minutes. Among the biochars, BC-700 exhibits a marginally superior performance relative to BC-500 and BC-300, indicating a restricted capacity of biochar for nitrate adsorption (Zhao et al., 2017). In contrast, the removal of ammonium demonstrates a significant increase with extended contact time, with BC-700 achieving the highest removal efficiency of around 52% at 180 minutes, followed closely by BC-500 at approximately 50% and BC-300 at about 45%. This variation can be attributed to the greater surface area and microporosity associated with biochars produced at higher pyrolysis temperatures (Ahmad et al., 2014; Keiluweit et al., 2010). Similarly, the removal of phosphorus enhances with prolonged contact time, with BC-700 again reaching the highest efficiency at roughly 52% at 180 minutes, followed by BC-500 at around 50% and BC-300 at approximately 48%. This improvement is likely due to the presence of mineral constituents such as calcium and magnesium oxides, which facilitate phosphorus retention (Xu et al., 2017). These findings suggest that biochars generated at elevated pyrolysis temperatures possess enhanced adsorption capabilities for ammonium and phosphorus, while the low efficiency of nitrate removal indicates that supplementary treatment strategies may be required for effective nitrate remediation (Zhao et al., 2013).

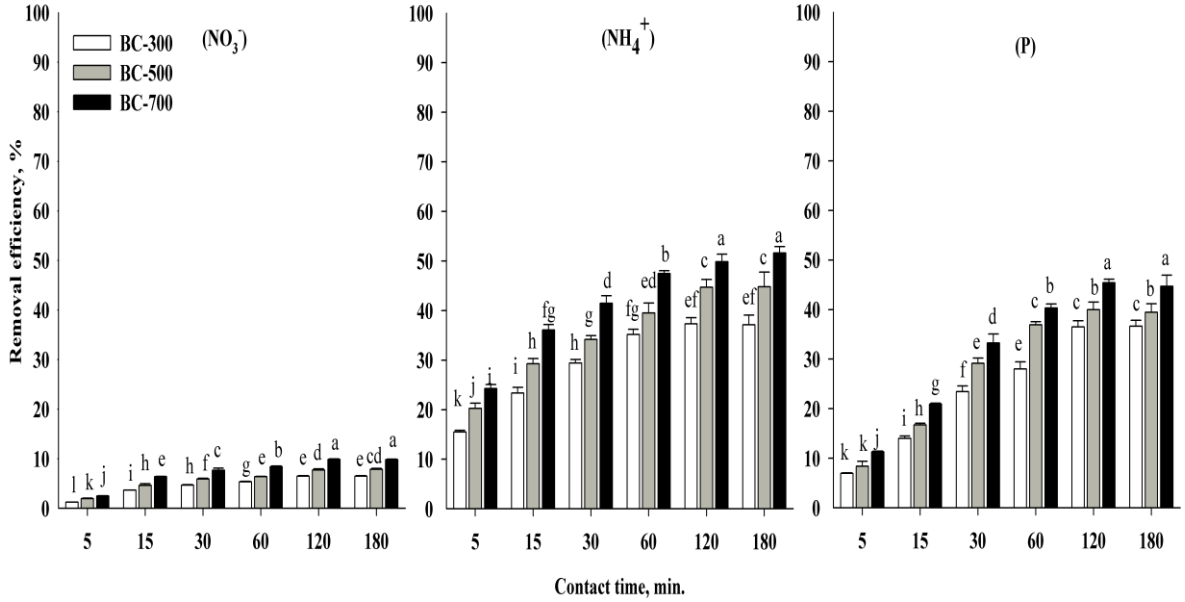

Figure 3. Effect contact time on NO_3^-, NH_4^+ and P ions removal by using BC-300, BC-500 and BC-700, concentration 50 mg L^{-1}, adsorbent dosage 1.0 g L^{-1} and the agitation was carried out at room temperature and 120 rbm.

3.2.2. Sorbent dosage

Figure 4. presents the influence of sorbent dosage (ranging from 0.5 to 10 g L^{-1}) on the removal efficiency of NO_3^-, NH_4^+ and P from aqueous solutions utilizing biochars produced at varied pyrolysis temperatures (300°C, 500°C and 700°C). The results reveal that the removal efficiency for all three pollutants enhances with an increase in biochar dosage; however, the degree of improvement differs among the pollutants and types of biochar employed. Specifically, NO_3^- removal remains comparatively low across all biochar dosages, with BC-700 demonstrating the highest efficiency (approximately 35% at 10 g L^{-1}), followed by BC-500 (approximately 30%) and BC-300 (approximately 25%). This observation implies that biochar possesses a limited affinity for nitrate adsorption, likely attributable to its anionic characteristics and the electrostatic repulsion encountered from negatively charged biochar surfaces (Zhao et al., 2017). In contrast, NH_4^+ removal exhibits a notable dose-dependent increase, with BC-700 achieving the highest removal rate (approximately 70% at 10 g L^{-1}), succeeded by BC-500 (around 65%) and BC-300 (approximately 60%). This phenomenon can be ascribed to cation exchange interactions and an increased adsorption capacity associated with elevated pyrolysis temperatures (Ahmad et al., 2014; Keiluweit et al., 2010). In addition, the stronger affinity of NH_4^+ ions for the negatively charged surfaces of biochar, which is influenced by the biochar's surface chemistry and cation exchange capacity (CEC) (Yao et al., 2012). Phosphorus removal also demonstrates a robust positive correlation with biochar dosage, wherein BC-700 achieves close to 80% removal at 10 g L^{-1}, surpassing BC-500 (about 75%) and BC-300 (approximately 70%). The enhanced performance of high-temperature biochars for ammonium and phosphorus adsorption is likely due to the development of a highly porous structure, augmented surface area, and the presence of mineral phases such as calcium and magnesium oxides that facilitate phosphate precipitation (Xu et al., 2018). These findings indicate that increasing biochar dosage significantly bolsters pollutant removal, particularly concerning NH_4^+ and P, while NO_3^- removal remains constrained, necessitating alternative remediation strategies (Zhao et al., 2017).

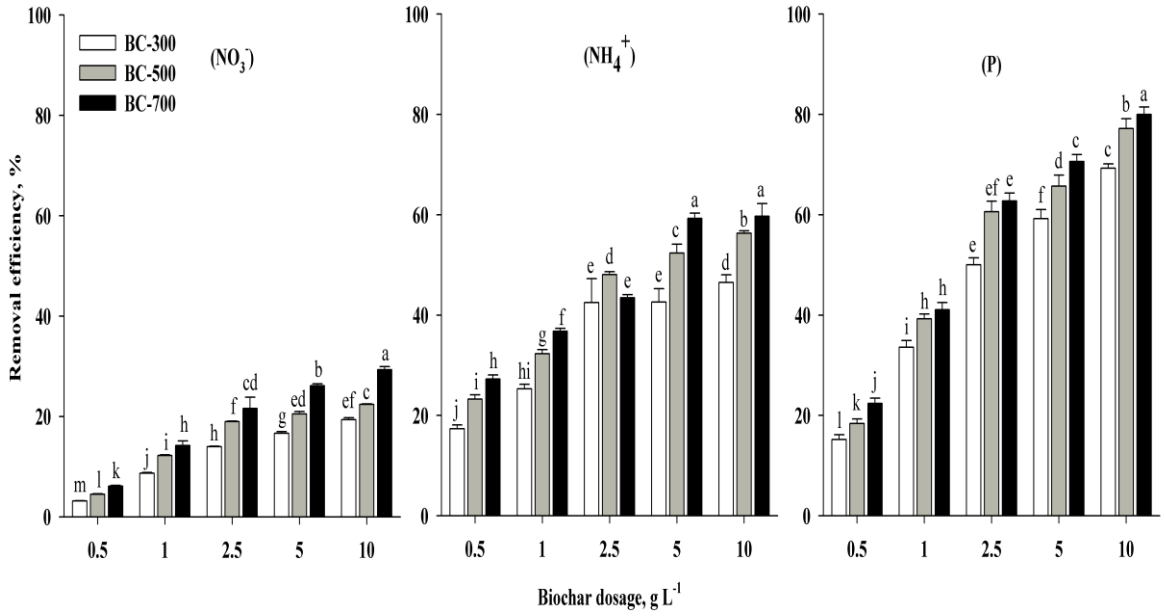

Figure 4. Effect sorbent dosage on NO_3^-, NH_4^+ and P ions removal by using BC-300, BC-500 and BC-700, concentration 50 mg L^{-1} and the agitation was carried out at room temperature and 120 rbm.

3.3 . Adsorption isotherms

Data presented in Table 2. And figure 5 shows adsorption isotherms of NO_3^-, NH_4^+ and P by using the tested biochars. The study investigated the adsorption of NO_3^-, NH_4^+, and P from aqueous solutions utilizing biochars produced through pyrolysis at temperatures of 300°C, 500°C, and 700°C. The analysis employed Langmuir and Freundlich isotherm models, which highlighted notable variations in adsorption capacity and underlying mechanisms. In the case of nitrate, the Freundlich model exhibited superior fitting ($R^2 > 0.987$) relative to the Langmuir model ($R^2 < 0.272$), with the maximum adsorption capacity (qmax) increasing from 0.47587 mg g^{-1} for biochar produced at 300°C (BC-300) to 1.53116 mg g^{-1} for biochar produced at 700°C (BC-700). This trend indicates an augmented adsorption capacity at elevated pyrolysis temperatures, likely attributable to enhancements in surface area and porosity, although the adsorption intensity (Kf) diminished from 4470.95 to 1190.15, potentially due to alterations in surface chemistry (Yuan et al., 2011). Similarly, for ammonium, the Freundlich model displayed an excellent fit ($R^2 > 0.976$), with qmax rising from 6.68896 mg g^{-1} for BC300 to 14.245 mg g^{-1} for BC-700. This finding suggests an enhanced adsorption capacity at higher temperatures, likely due to an increase in cation exchange capacity (CEC), while Kf decreased from 410.20 to 237.08, indicating a reduction in adsorption intensity (Yao et al., 2012). Regarding P, the Freundlich model also yielded a strong fit ($R^2 > 0.957$), with qmax increasing from 10.2041 mg g^{-1} for BC-300 to 14.4092 mg g^{-1} for BC500, and remaining constant for BC-700. This stability is likely due to the formation of metal oxides that facilitate phosphorous binding, while Kf decreased from 378.53 to 227.35, illustrating a decrease in adsorption intensity. Overall, the findings suggest that higher pyrolysis temperatures enhance the adsorption capacity for all evaluated nutrients, albeit with a concurrent decrease in adsorption intensity. Furthermore, the Freundlich model consistently demonstrated a superior fit, indicating heterogeneous adsorption surfaces and intricate mechanisms at play (Yuan et al., 2011; Yao et al., 2012).

Table 2. Freundlich and Langmuir adsorption isotherm for NO_3^-, MH_4^+ and P ions adsorption onto tested biochars

Biochar	Langmuir					Freundlich				
	Slope	Intercept	R^2	Qmax (mg g^{-1})	**b, (L mg^{-1})**	n	Kf	Slope	Intercept	R^2
					NO_3^-					
BC-300	-2.101	77.869	0.229	0.476	0.027	2.691	4470.952	0.372	3.650	0.991
BC-500	-1.218	48.990	0.272	0.821	0.025	2.466	2740.312	0.406	3.438	1.000
BC-700	-0.653	32.664	0.268	1.531	0.020	2.122	1190.145	0.471	3.076	0.988
					NH_4^+					
BC-300	-0.150	13.824	0.298	6.689	0.011	2.575	410.204	0.388	2.613	0.993
BC-500	-0.089	9.388	0.309	11.249	0.009	2.682	298.745	0.373	2.475	0.977
BC-700	-0.070	7.721	0.329	14.245	0.009	2.710	237.083	0.369	2.375	0.989
					P					
BC-300	-0.098	10.456	0.318	10.204	0.009	3.023	378.530	0.331	2.578	0.995
BC-500	-0.069	7.941	0.319	14.409	0.009	3.000	257.158	0.333	2.410	0.975
BC-700	-0.058	7.005	0.308	14.245	0.010	3.258	227.353	0.307	2.357	0.957

3.4 Kinetics of sorption

Table 3 and figure 6 presents the kinetics of sorption for NO_3^-, NH_4^+ and P onto biochars produced through pyrolysis at temperatures of 300°C, 500°C, and 700°C were investigated using both pseudo-first-order and pseudo-second-order models. This analysis elucidated the underlying mechanisms and rates of adsorption. For NO_3^-, the pseudo-first-order model exhibited a superior fit ($R^2 > 0.963$) in comparison to the pseudo-second-order model ($R^2 < 0.934$), with rate constants (K_1) ranging from 0.121 to 0.151 min^{-1}. This suggests that physical adsorption phenomena, such as diffusion, likely predominated the process. The equilibrium adsorption capacity (qe) remained fairly consistent across the different biochars, averaging approximately 49–50 mg g^{-1}, indicating that variations in pyrolysis temperature had a negligible impact on nitrate adsorption capacity. In relation to NH_4^+, the pseudo-second-order model demonstrated an excellent fit ($R^2 > 0.991$), with rate constants (K_2) spanning 2.221 to 3.265 g/mg min^{-1}, suggesting that chemisorption mechanisms, such as ion exchange or surface complexation, were primarily responsible. Notably, the qe values exhibited a significant increase with rising pyrolysis temperature, escalating from 87.418 mg g^{-1} for BC-300 to 168.888 mg g^{-1} for BC-700, likely attributable to enhanced cation exchange capacity (CEC) and increased surface area associated with higher pyrolysis temperatures (Yao et al., 2012). For P, the pseudo-first-order model achieved a better fit ($R^2 > 0.924$) than the pseudo-second-order model ($R^2 < 0.973$), with K_1 values rising from 0.536 to 0.809 min^{-1}, thus indicating that physical adsorption, including pore diffusion, played an important role. Additionally, the qe values for phosphorus increased with pyrolysis temperature, from 64.789 mg g^{-1} for BC300 to 85.114 mg g^{-1} for BC-700, likely due to the generation of metal oxides and an increased surface area which enhanced phosphorus binding (Yuan et al., 2011).

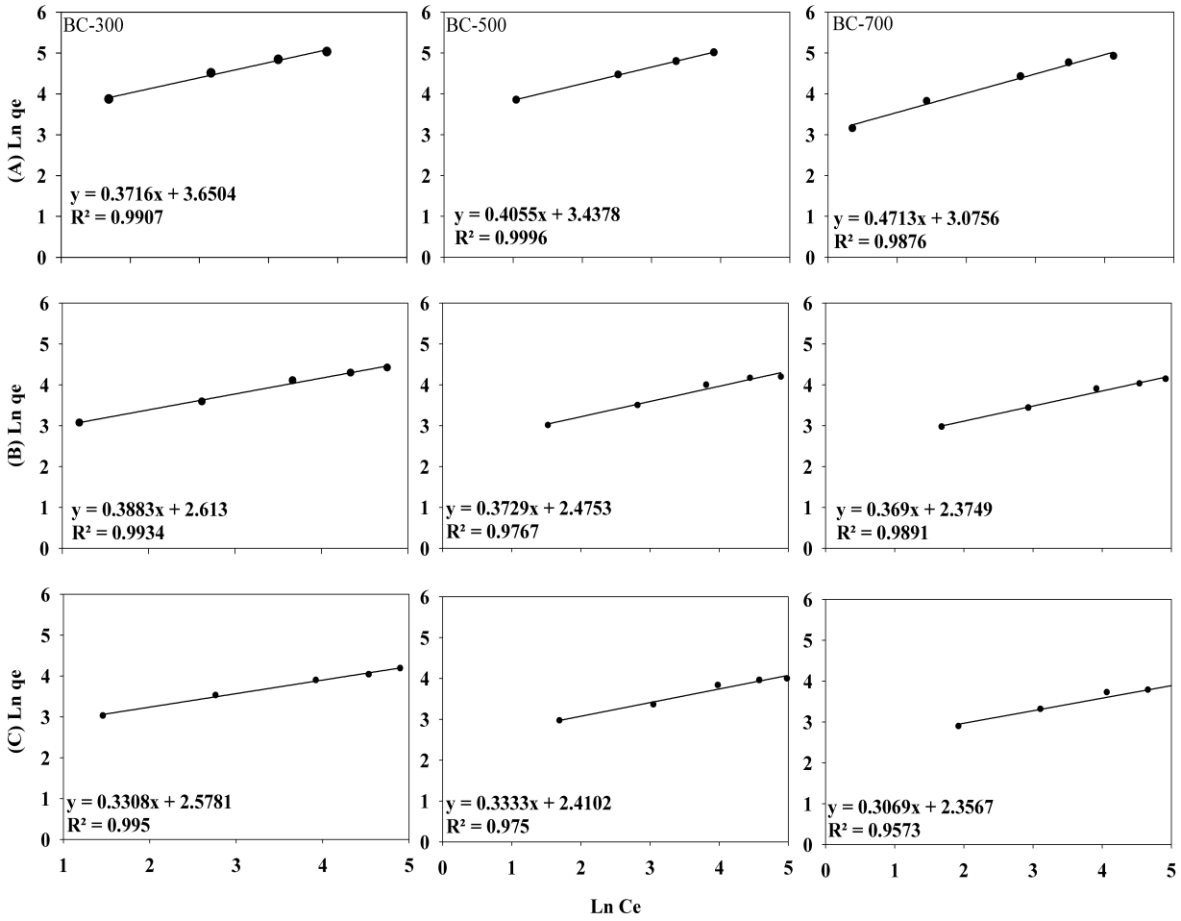

Figure 5. Freundlich isotherm models for NO_3^- (A), NH_4^+ (B) and P (C) adsorption onto tested biochars

In summary, the findings illustrate that the mechanisms of adsorption varied with the type of nutrient, NO_3^- adsorption was predominantly physical, NH_4^+ adsorption was primarily chemisorption-driven, and P adsorption entailed a combination of both physical and chemical processes. Increased pyrolysis temperatures generally augmented adsorption capacities for ammonium and phosphorus, while exerting limited effects on nitrate, thereby underlining the necessity of optimizing biochar properties for targeted nutrient removal applications (Yao et al., 2012; Yuan et al., 2011).

4. Conclusions

This study illustrates that the biochar derived from date palm petiole at varying pyrolysis temperatures displays differing adsorption efficiencies for NO_3^-, NH_4^+, and P in aqueous solutions. Elevated pyrolysis temperatures enhanced the adsorption of NH_4^+ and P, attributed to improvements in surface area, porosity, and cation exchange capacity, with BC-700 achieving the highest level of adsorption capacity. Conversely, NO_3^- removal remained consistently low across all biochar samples, indicating a limited capacity for electrostatic interactions and adsorption affinity. The adsorption of NO_3^- and P was best characterized by the pseudo-first-order model, whereas NH_4^+ adsorption adhered to a pseudo-second-order model, suggesting that chemisorption was the predominant mechanism for ammonium uptake. The Freundlich isotherm model yielded the most accurate representation of the adsorption process, reflecting the presence of heterogeneous sorption sites. While biochar emerges as a promising material for nutrient recovery, it is imperative to optimize its properties and explore potential modifications to enhance nitrate removal efficacy. Future investigations

should concentrate on biochar amendments, incorporation of co-adsorbents, and the application in real wastewater scenarios to further elevate its practical utility in sustainable wastewater treatment systems.

Table 3. Kinetic parameters obtained from pseudo-first-order and pseudo-second-order for NO_3^-, NH_4^+ and P adsorption by tested biochars.

Biochar	Pseudo-first order					Pseudo-second order				
	Slope	**Intercept**	**R^2**	**K1**	**qe**	**Slope**	**Intercept**	**R^2**	**K2**	**qe**
					NO_3^-					
BC-300	-0.052	1.697	0.992	0.121	49.774	-20.940	14.328	0.792	30.603	-0.048
BC-500	-0.066	1.703	0.993	0.151	50.443	-17.010	12.318	0.934	23.489	-0.059
BC-700	-0.056	1.695	0.963	0.128	49.522	-13.571	10.115	0.761	18.208	-0.074
					NH_4^+					
BC-300	-0.346	1.942	0.975	0.796	87.418	-3.112	3.873	0.999	2.501	-0.321
BC-500	-0.470	2.084	0.970	1.081	121.367	-0.321	4.608	0.991	3.265	-0.258
BC-700	-0.589	2.228	0.971	1.355	168.888	-2.734	3.367	0.994	2.221	-0.366
					P					
BC-300	-0.233	1.812	0.924	0.536	64.789	-2.965	5.059	0.892	1.738	-0.337
BC-500	-0.276	1.850	0.946	0.635	70.746	-1.745	3.409	0.963	0.893	-0.573
BC-700	-0.351	1.930	0.946	0.809	85.114	-2.224	3.670	0.973	1.348	-0.450

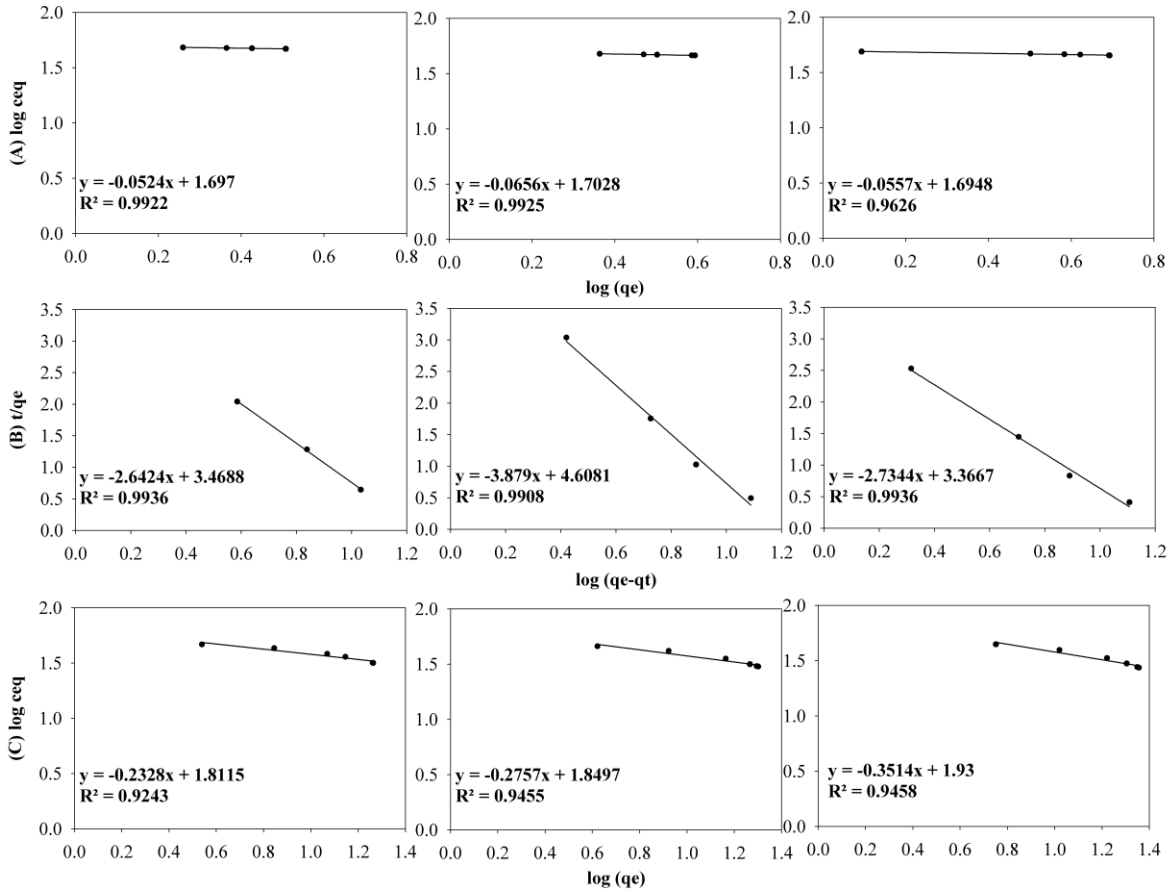

Figure 6. Pseudo-first-order kinetics for NO_3^- (A) and P (C) and pseudo-second-order kinetic for NH_4^+ (B) ions adsorption onto tested biochars.

Author Contributions

Conceptualization, and supervision A.A.A, and K.M.I; methodology, B.M.K., A.A.A.; software, K.M.I.; validation, A.A.A and K.M.I.; formal analysis, investigation, resources, data curation, writing -initial draft preparation, writing, reviewing and editing, B.M.K., A.A.A., and K.M.I. The final paper has been reviewed and approved by all authors.

Acknowledgments

This study was supported by the Academy of Scientific Research and Technology, Energy, Environment and Water Nexus (ASRT-APPLE), project number (9112).

Conflicts of Interest

The authors declare no conflict of interest.

References

Abdelhafez, A.A., & Li, J. (2016). Removal of Pb(II) from aqueous solution by using biochars derived from sugar cane bagasse and orange peel. Journal of the Taiwan Institute of Chemical Engineers. 61, 367-375. https://doi.org/10.1016/j.jtice.2016.01.005

Abdelhafez, A.A., Li, J., Mohamed H.H. Abbas. (2014). Feasibility of biochar manufactured from organic wastes on the stabilization of heavy metals in a metal smelter contaminated soil. Chemosphere. 117, 66-71. https://doi.org/10.1016/j.chemosphere.2014.05.086

Abdelhafez, A.A., Zhang, X., Zhou, L., Cai, M., Cui, N., Chen, G., Zou, G., Abbas, M.H.H., Kenawy, M.H.M., Ahmad, M. Alharthi, S.S., & Hamed, M.H. (2021). Eco-friendly production of biochar via conventional pyrolysis: Application of biochar and liquefied smoke for plant productivity and seed germination. Environmental Technology and Innovation. 22, 101540. https://doi.org/10.1016/j.eti.2021.101540

Abdelhafez, A.A., Zhanga, X., Zhou, L., Zou, G., Cui, N., Abbas, M.H.H., & Hamed, M.H. (2020). Introductory Chapter: Is Biochar Safe? Applications of Biochar for Environmental Safety, Ahmed A. Abdelhafez and Mohammed H. H. Abbas, IntechOpen, DOI: 10.5772/intechopen.91996. Available from: https://www.intechopen.com/chapters/71729

Aghoghovwia, M.P., Hardie, A.G., & Rozanov, A.B. (2022). Characterisation, adsorption and desorption of ammonium and nitrate of biochar derived from different feedstocks. Environmental Technology. 43(5), 774-787. https://doi.org/10.1080/09593330.2020.1804466

Ahmad, M., Rajapaksha, A. U., Lim, J. E., Zhang, M., Bolan, N., Mohan, D., Meththika Vithanage, M., Lee, S.S., & Ok, Y. S. (2014). Biochar as a sorbent for contaminant management in soil and water: A review. Chemosphere. 99, 19-33. https://doi.org/10.1016/j.chemosphere.2013.10.071

Akhtar, L., Ahmad, M., Iqbal, S., Abdelhafez, A.A., & Mehran, M.T. (2021). Biochars' adsorption performance towards moxifloxacin and ofloxacin in aqueous solution: Role of pyrolysis temperature and biomass type. Environmental Technology and Innovation. 24, 101912. https://doi.org/10.1016/j.eti.2021.101912

Chatterjee, R., Sajjadi, B., Chen, W-Y., Mattern, D.L., Hammer, N., Raman, V. & Dorris, A. (2020). Effect of pyrolysis temperature on physicochemical properties and acoustic-

based amination of biochar for efficient CO_2 adsorption. Front. Energy Res. 8, 85. doi: 10.3389/fenrg.2020.00085

Chen, B., Zhou, D., & Zhu, L. (2008). Transitional adsorption and partition of nonpolar and polar aromatic contaminants by biochars of pine needles with different pyrolytic temperatures. Environ. Sci. Technol. 42(14), 5137–5143. https://doi.org/10.1021/es8002684

Gai, X., Wang, H., Liu, J., Zhai, L., Liu, S., Ren, T., & Liu, H. (2014). Effects of feedstock and pyrolysis temperature on biochar adsorption of ammonium and nitrate. PLoS One. 9(12), e113888. https://doi.org/10.1371/journal.pone.0113888

Ho, Y.S., & McKay, G. (1999). The sorption of lead(II) ions on peat. Water Res. 33, 578-84. https://doi.org/10.1016/S0043-1354(98)00207-3

Inyang, M., Gao, B., Yao, Y., Xue, Y., Zimmerman, A., Pullammanappallil, P., & Cao, X. (2012). Removal of heavy metals from aqueous solution by biochar produced from anaerobically digested sugarcane bagasse. Bioresource Technology. 110, 50-56. https://doi.org/10.1016/j.biortech.2012.01.072

Joo, J.H., Hassan, S.H.A., & Oh, S.E. (2010). Comparative study of biosorption of Zn^{2+} by Pseudomonas aeruginosa and Bacillus cereus. Int Biodeterior Biodegrad. 64, 734-41. https://doi.org/10.1016/j.ibiod.2010.08.007

Keiluweit, M., Nico, P. S., Johnson, M. G., & Kleber, M. (2010). Dynamic molecular structure of plant-derived black carbon (biochar). Environmental Science & Technology. 44(4), 1247-1253. https://doi.org/10.1021/es9031419

Khater, E.S., Bahnasawy, A., Hamouda, R., Sabahy, A., Abbas, W., & Morsy, O.M. (2024). Biochar production under different pyrolysis temperatures with different types of agricultural wastes. Sci Rep 14, 2625. https://doi.org/10.1038/s41598-024-52336-5

Liu, Z., Dugan, B., Masiello, C. A., & Gonnermann, H. (2017). Biochar particle size, shape, and porosity act together to influence soil water properties. PLoS One. 14(6), e0215024. https://doi.org/10.1371/journal.pone.0215024

Nan, H., Yin, J., Yang, F., Luo, Y., Zhao, L., & Cao, X. (2021). Pyrolysis temperature-dependent carbon retention and stability of biochar with participation of calcium: Implications to carbon sequestration. Environmental Pollution. https://pdfs.semanticscholar.org/7cea/e60ff81fc704e3a9b5d9e7cb357179f76c86.pdf

Paerl, H.W., & Paul, V.J. (2011). Climate change: Links to global expansion of harmful cyanobacteria. Water Research. 46(5), 1349-1363. https://doi.org/10.1016/j.watres.2011.08.002

Smith, V.H., Tilman, G.D., & Nekola, J.C. (1999). Eutrophication: Impacts of excess nutrient inputs on freshwater, marine, and terrestrial ecosystems. Environmental Pollution. 100(1-3), 179-196. https://doi.org/10.1016/S0269-7491(99)00091-3

Tan, I.A.W., Ahmad, A.L., & Hameed, B.H. (2008). Adsorption isotherms, kinetics, thermodynamics and desorption studies of 2,4,6-trichlorophenol on oil palm empty fruit bunch-based activated carbon. Journal of Hazardous Materials. 164, 473-82. https://doi.org/10.1016/j.jhazmat.2008.08.025

Tan, X., Liu, Y., Zeng, G., Wang, X., Hu, X., Gu, Y., & Yang, Z. (2015). Application of biochar for the removal of pollutants from aqueous solutions. Chemosphere. 125, 70-85. https://doi.org/10.1016/j.chemosphere.2014.12.058

Tomczyk, A., Sokołowska, Z. & Boguta, P. (2020). Biochar physicochemical properties: pyrolysis temperature and feedstock kind effects. Rev Environ Sci Biotechnol. 19, 191–215. https://doi.org/10.1007/s11157-020-09523-3

Vijayaraghavan, K. & Balasubramanian, R. (2021). Application of pinewood waste-derived biochar for the removal of nitrate and phosphate from single and binary solutions. Chemosphere. Volume 278, 130361. https://doi.org/10.1016/j.chemosphere.2021.130361

Wang, Y., Song, X., Xu, Z. Cao, X., Song, J., Huang, W., Ge, X., & Wang, H. (2021). Adsorption of nitrate and ammonium from water simultaneously using composite adsorbents constructed with functionalized biochar and modified zeolite. Water Air Soil Pollut. 232, 198. https://doi.org/10.1007/s11270-021-05145-9

Ward, M.H., deKok, T.M., Levallois, P., Brender, J., Gulis, G., Nolan, B.T., & VanDerslice, J. (2005). Workgroup report: Drinking-water nitrate and health-Recent findings and research needs. Environmental Health Perspectives. 113(11), 1607-1614. https://doi.org/10.1289/ehp.8043

Xiao, J., Long, H., He, X., Chen, G., Yuan, T., Liu, Y., & Xu, Q. (2024). Synthesis of MgO-coated canna biochar and its application in the treatment of wastewater containing phosphorus. Water. 16, 873. https://doi.org/10.3390/w16060873

Xu, X., Cao, X., Zhao, L. Wang, H., Yu, H., & Gao, B. (2013). Removal of Cu, Zn, and Cd from aqueous solutions by the dairy manure-derived biochar. Environ Sci Pollut Res 20, 358–368. https://doi.org/10.1007/s11356-012-0873-5

Xu, X., Zhao, Y., Sima, J., Zhao, L., Mašek, O., & Cao, X. (2017). Indispensable role of biochar-inherent mineral constituents in its environmental applications: A review. Bioresource Technology. 241, 887-899. https://doi.org/10.1016/j.biortech.2017.06.023

Yao, Y., Gao, B., Zhang, M., Inyang, M., & Zimmerman, A.R. (2012). Effect of biochar amendment on sorption and leaching of nitrate, ammonium, and phosphate in a sandy soil. Chemosphere. 89(11), 1467-1471. https://doi.org/10.1016/j.chemosphere.2012.06.002

Yuan, J. H., Xu, R. K., & Zhang, H. (2011). The forms of alkalis in the biochar produced from crop residues at different temperatures. Bioresource Technology. 102(3), 3488–3497. https://doi.org/10.1016/j.biortech.2010.11.018

Zhang, Z., Huang, G., Zhang, P., Shen, J., Wang, S., & Li, Y. (2023). Development of iron-based biochar for enhancing nitrate adsorption: Effects of specific surface area, electrostatic force, and functional groups. Science of The Total Environment, 856, 159037. https://doi.org/10.1016/j.scitotenv.2022.159037

Zhao, L., Cao, X., Masek, O., & Zimmerman, A. (2013). Heterogeneity of biochar properties as a function of feedstock sources and production temperatures. Journal of Hazardous Materials. 256-257, 1-9. https://doi.org/10.1016/j.jhazmat.2013.04.015

Zhao, L., Cao, X., Masek, O., & Zimmerman, A. (2017). Heterogeneity of biochar properties as a function of feedstock sources and production temperatures. Journal of Hazardous Materials. 256-257, 1-9. https://doi.org/10.1016/j.jhazmat.2013.04.015